THE ASTROPHYSICAL JOURNAL, 557:605–615, 2001 August 20

HIGH-REDSHIFT GALAXY OUTFLOWS AND THE FORMATION OF DWARF GALAXIES

EVAN SCANNAPIECO, ROBERT J. THACKER, AND MARC DAVIS
Department of Astronomy, University of California, Berkeley, CA 94720
Received 2000 November 13; accepted 2001 April 24

ABSTRACT

We examine the effects of galaxy outflows on the formation of dwarf galaxies in numerical simulations of the high-redshift universe. Using a smoothed particle hydrodynamic code, we conduct two detailed simulations of a (5.2 Mpc h^{-1})^3 comoving volume of the universe. In both simulations we implement simple, well-motivated models of galaxy identification and star formation, while our second simulation also includes a simple "blow-out" model of galaxy outflows in which supernova driven winds from newly formed disk galaxies punch out and shock the intergalactic medium while leaving the host galaxies intact. A direct comparison between these simulations suggests that there are two major mechanisms by which outflows affect dwarf formation. First, the formation of an outflow slows down the further accretion of gas onto a galaxy, causing an overall decrease of approximately 50% in the total gas mass accreted by the objects in our simulations. Additionally, our simulations uncover a significant population of $\sim 10^9$ $M_\odot$ objects whose formation is suppressed by the mechanism of "baryonic stripping," in which outflows from early galaxies strip the gas out of nearby overdense regions that would have otherwise later formed into dwarf galaxies. This mechanism may be important in explaining the observed discrepancy between the number of dwarf galaxies predicted and observed in the local group and provide a natural explanation for the formation of empty halos which may be required by the existence of the extremely gas-poor extragalactic high-velocity clouds.

Subject headings: cosmology: theory — galaxies: formation — intergalactic medium

1. INTRODUCTION

It has long been recognized that the properties of the diffuse gas within clusters of galaxies are indicative of a violent past. The slope of the X-ray luminosity-temperature relationship of the hot intracluster medium in galaxy clusters is far too steep to be due to heating only by virializing shocks, requiring that large quantities of heated material be injected into this gas at early times. (see, e.g., Kaiser 1991; Mushotzky & Scharf 1997; Eke, Navarro, & Frenk 1998; Cavaliere, Menci, & Tozzi 1999). Similarly, the metallicity of the intracluster medium is observed to be quite high, ~ 0.3 $Z_\odot$, and constant over a large range of cluster masses (Renzini 1997), indicating widespread enrichment by material ejected by supernovae. (For an alternative viewpoint, see Bryan 2000 and Pearce et al. 2000).

While the first observational evidence for preheating and enrichment was met with theoretical resistance, hindsight leads us to believe that we might have expected this all along. As structure formation is thought to occur hierarchically, and this growth is biased to the same overdense regions at all times, it is natural to expect that a large population of dwarf galaxies would have once been found near the locations of present-day clusters. It has also been widely observed that dwarf galaxies undergo outflows both at low and high redshift. Several studies of expanding H I gas in nearby dwarf galaxies show clear evidence of dense, expanding shells with velocities above 15 km s^{-1} (Marlowe et al. 1995; Heckman 1997; Martin 1998) as well as halos of hot ($\sim 5 \times 10^6$ K) gas surrounding these objects (della Ceca et al. 1996; Bomans, Chu, & Hopp 1997). Similarly, spectroscopic studies of galaxies have confirmed that high-velocity winds are present around dwarf galaxies at redshifts ~ 3 (Pettini et al. 1998; Pettini 2001) and even higher (Frye & Broadhurst 1998; Warren et al. 1998). Taken together these observational facts suggest a picture in which outflows powered by starbursts in the earliest dwarf galaxies had a huge impact on the properties of the gas that later condensed within clusters of galaxies.

Thus, a vague theoretical scheme exists for understanding the preheating of clusters; yet surprisingly, the impact of this mechanism on the intergalactic medium (IGM) has been largely unexplored. Although clusters and galaxies both condense out of the same material, preheating is only considered in cluster simulations (see, e.g., Metzler & Evrard 1994; Yepes et al. 1997) and simulations of the properties of the IGM (Nath & Trentham 1997; Madau, Ferrara, & Rees 2000), while all numerical galaxy formation simulations carried out to date assume primordial conditions. Feedback in these simulations is modeled solely as impacting the interstellar medium within the galaxy, without affecting the IGM and neighboring galaxy formation.

We have recently conducted two exploratory semianalytical studies on the impact of galaxy outflows on the IGM and the formation of galaxies within it (Scannapieco, Ferrara, & Broadhurst 2000; Scannapieco & Broadhurst 2001, hereafter SB). These studies have shown that outflows may be crucial in resolving such long-standing astronomical mysteries as the factor of 4 discrepancy between the number of observed and predicted Milky Way Satellite galaxies (see, e.g., Klypin et al. 1999; Moore et al. 1999) and the physical processes that cause elliptical galaxies to be typically much larger than disks (see, e.g., Bromley et al. 1998). The results of our semianalytic simulations hinged on the importance of a mechanism of "baryonic stripping" in which outflows from early galaxies strip the gas out of nearby overdense regions of the IGM that would have otherwise later formed into dwarf galaxies.

In SB we were able to illustrate the importance of this mechanism in an idealized context; however, the nonlinear clustering of galaxies, complicated evolution of outflows, and details of shock motion through collapsing regions can

be captured only through numerical simulation. In this article we address this question in the more detailed setting of smoothed particle hydrodynamic (SPH) simulations, studying the impact of a simple model of galaxy outflows on the formation of structure in a typical volume of the universe.

Feedback has been implemented by other authors using a number of different prescriptions. The lack of a fundamental theory of star formation and the interstellar medium render it extremely difficult to decide how to model star formation and feedback "correctly." For example, the dispersal of energy from supernovae can be achieved by thermal heating, by passing kinetic energy to the gas, or by some arbitrary combination of the two. Katz (1992) was the first to consider the effect of thermal heating, and this seminal work highlighted a fundamental problem, namely that the cooling time for hot dense gas is so short (less than a Myr) that simply returning feedback energy as thermal heating has little effect. Navarro & White (1993) considered a feedback model with both kinetic boosts and thermal heating. Mihos & Hernquist (1994) and Gerritsen (1997) have studied the effect of feedback modeled as kinetic boosts in isolated disk galaxies. Gerritsen has argued that the boost model is too efficient when energy transfer parameters are chosen to match theoretical predictions such as those of Thornton et al. (1998). This is probably related to the fact that the kinetic energy boosts are calculated using a fixed energy budget that does not account for the force softening that occurs at the short scales on which feedback is modeled.

More recently, Yepes et al. (1997) have constructed a multiphase model of star formation and feedback, which has been implemented in SPH simulations by Hultman & Pharasyn (1999). Given the large number of uncertainties in modeling the evolution of the interstellar medium, it remains unclear if such sophisticated approaches are well motivated. Thacker & Couchman (2000) present a number of different approaches to modeling feedback, including a new approach where drastic radiative losses are prevented by using a modified cooling formalism. Springel (2000) has developed a model where the local evolution of gas can become dominated by turbulent pressure support from exploding supernovae. A survey of the current status of feedback in simulations of galaxy formation can be found in Thacker & Davis (1999).

Given the inherent difficulty in modeling feedback, in this work we adopt a simple kinetic model that is inspired by the numerical simulations conducted by Mac Low & Ferrara (1999) and Ferrara & Tolstoy (2000). Here the authors demonstrate that in disk galaxies within halos of $10^7\ M_\odot \lesssim M \lesssim 10^9\ M_\odot$, a "blow-out" occurs in which superbubbles formed by groups of Type II supernovae punch out of the disk, shocking the IGM while leaving the interstellar medium of the galaxy intact. This is due to the fact that while supernovae are inefficient at ejecting material within the disk, they expand almost freely in the perpendicular direction, resulting in a large organized wind made up of mostly the gas surrounding the galaxy. This scenario has also been supported by the numerical simulations of Martel & Shapiro (2001).

The structure of this work is as follows. In § 2 we outline the numerical method adopted and the simplifying assumptions used in constructing our model for galaxy outflows. In § 3 we compare the results from hydrodynamic simulations conducted both with and without outflows to examine the impact of outflows on the number density and distribution of galaxies of varying mass scales. Conclusions are given in § 4.

2. SIMULATING GALAXY OUTFLOWS

2.1. *Overview of the Numerical Method*

We model the gravitational and hydrodynamic forces using a particle-based method. The gravitational interactions are calculated using the adaptive particle-particle, particle-mesh (AP^3M) algorithm of Couchman (1991), while hydrodynamic forces are calculated using smoothed particle hydrodynamics (Gingold & Monaghan 1977; Lucy 1977). We use a parallel OpenMP based implementation of the "HYDRA" code (Couchman, Thomas, & Pearce 1995; Thacker & Couchman 2000) that is optimized for execution on RISC processors.

Since we are attempting to calculate ensemble quantities, it is necessary for us to consider a uniform region of space that is not subject to bias due to the incorporation of a dominant collapse mode. We must also ensure that the mass resolution is sufficient to be able to resolve groups of mass $10^8\ M_\odot$, the smallest mass that can cool effectively without molecular cooling or in the presence of an ionizing background (see, e.g., Haiman, Rees, & Loeb 1997; Ciardi et al. 2000; SB).

These criteria, along with those of wall clock limitations, have lead us to use a periodic box of size $5.2\ h^{-1}$ Mpc and a particle number of 2×192^3. The use of such a small box precludes evolving to low redshift, but this is not a concern since we are interested in the formation epoch of low ($<10^{10}\ M_\odot$) mass halos. The mass resolution in the dark matter is $2.5 \times 10^6\ M_\odot$, while that within the gas is $5 \times 10^5\ M_\odot$, rendering a $2 \times 10^8\ M_\odot$ halo resolved by 80 particles. We use a fixed physical Plummer softening length of 1.54 kpc, which leads to minimum hydrodynamic scale of $h_{\rm min} = 1.8$ kpc.

A detailed discussion of the SPH solver used in this investigation is given by Thacker et al. (2000). Here we discuss features of the algorithm that intimately relate to the group identification scheme and outflow processes we are modeling.

The density at a given point within the simulation is given by

$$\langle \rho(\boldsymbol{r}_i) \rangle = \sum_{j=1, r_{ij}<2h_i}^{N} m_j [W(\boldsymbol{r}_i - \boldsymbol{r}_j, h_i) + W(\boldsymbol{r}_i - \boldsymbol{r}_j, h_j)]/2 \ , \tag{1}$$

where $W(\boldsymbol{r}, h)$ is the (B_2 spline) SPH smoothing kernel, h_i is the smoothing length associated with particle i, m_j is the mass of particle j, and $\boldsymbol{r}_i$ and $\boldsymbol{r}_j$ are the coordinates of particles i and j, with r_{ij} the distance between them. The arithmetic average of the kernels is used to ensure that the equation of motion is correct to order ∇h, when used in combination with the gather-only neighbor finding method (see Thacker et al. 2000 for a careful discussion of this point). Hereafter we denote the arithmetic average of the kernels as $\overline{W}$.

The equation of motion is derived from the identity

$$\frac{\nabla P}{\rho} = \nabla \frac{P}{\rho} + \frac{P}{\rho^2} \nabla \rho \ , \tag{2}$$

where P is the pressure. Upon performing the standard SPH substitutions and making the following replacement,

$$\nabla_i \overline{W}(\boldsymbol{r}_i - \boldsymbol{r}_j, h_i, h_j) = -\nabla_j \overline{W}(\boldsymbol{r}_i - \boldsymbol{r}_j, h_j, h_i) + \mathcal{O}(\nabla h) , \quad (3)$$

this becomes (neglecting $\mathcal{O}(\nabla h)$ terms)

$$\frac{d\boldsymbol{v}_i}{dt} = \sum_{j=1}^{N} \frac{\boldsymbol{f}_{ij}}{m_i} = -\sum_{j=1, r_{ij}<2h_i}^{N} m_j \frac{P_i}{\rho_i^2} \nabla_i \overline{W}(\boldsymbol{r}_i - \boldsymbol{r}_j, h_i, h_j) + \sum_{j=1, r_{ij}<2h_j}^{N} m_j \frac{P_j}{\rho_j^2} \nabla_j \overline{W}(\boldsymbol{r}_i - \boldsymbol{r}_j, h_j, h_i) , \quad (4)$$

where $\boldsymbol{v}_i$ is the velocity of particle i and $\boldsymbol{f}_{ij}$ is the force on particle i due to particle j.

Finally, the energy equation used is that of Benz (1990),

$$\frac{d\epsilon_i}{dt} = \sum_{j=1, r_{ij}<2h_j}^{N} m_j \left(\frac{P_i}{\rho_i^2} + \frac{\Pi_{ij}}{2}\right)(\boldsymbol{v}_i - \boldsymbol{v}_j) \cdot \nabla_i \overline{W}(\boldsymbol{r}_i - \boldsymbol{r}_j, h_i, h_j) , \quad (5)$$

where ϵ_i is the internal energy of particle i and Π_{ij} is the artificial viscosity between the two particles. Note that while this equation is asymmetric in the particle indices, it still conserves energy to a high degree of accuracy. The single-sided approach is particularly helpful here since it prevents spurious heating and cooling of collapsed, dense objects. Radiative cooling is calculated for a constant 0.05 $Z_\odot$ metallicity gas, and the precise cooling table is interpolated from Sutherland & Dopita (1993). Because of the enormously fast change of cooling rates with temperature we calculate the exact amount of cooling using an integral formalism (see Thomas & Couchman 1992) that assumes a constant density over each time step.

2.2. *Identification of Dwarf Galaxies*

To study the impact of galaxy outflows on nearby density perturbations we must first know where and when a galaxy is formed in our simulations. As many of the objects of interest are at the limit of the resolution of the simulation, complex criteria that attempt to capture in detail the formation of massive stars in protogalaxies and the transfer of momentum from stellar winds and supernovae into galaxy outflows are not warranted. Such criteria inevitably introduce a number of parameters that affect the results in ways that are difficult to disentangle and inevitably subject to fine tuning. Thus, in this study we adopt a model that strives to be as simple as possible and parallels our previous semi-analytical work on this question (SB).

A common approach to object identification is to employ a friends-of-friends group finding algorithm, which links together all pairs of particles with separations less than some "linking length" r_L. While this technique has been widely tested and known to give good results (see, e.g., Davis et al. 1985; Lacy & Cole 1995) it is much too computationally expensive to implement regularly during a simulation.

Hence, we instead choose to identify collapsed protogalaxies by a simple density cut. Every 10 time cycles we find the most dense gas particle in each zone of the simulation that has not previously been identified as belonging to a galaxy and make a list of all zones in which these particles have overdensities above a threshold value, δ_c. To account for galaxies centered near zone edges, we exclude all zones with maximum densities lower than those of any of their neighbors. The points in the remaining zones are then taken to be candidates for the centers of new galaxies.

Around each of these points we sort all the neighboring baryonic particles according to their radial distance and continue to add particles (1, 2, 3, ... N) until $\delta_c \overline{\rho}_b \geq N m_g/(4\pi/3) r_N^3$, where m_g is the mass of each gas particles, and r_N is the distance from particle N to the center of the candidate galaxy. We then compute the center of mass of this configuration, resort the particles according to the distance from the center of mass and again add particles until $\delta_c \overline{\rho}_b \geq N m_g/(4\pi/3) r_N^3$. If the resulting object has a minimum mass of $2.5 \times 10^7\ M_\odot$ corresponding to 52 particles (the number of objects in the smoothing kernel of the SPH solver), the object is considered to be a galaxy with baryonic mass $m_g N$, otherwise the peak is below the resolution of the simulation and is ignored.

While this prescription is both easy to implement computationally and captures the essence of dwarf galaxy formation, it is important that we understand how it compares with more standard methods of object identification. To make this comparison, we have carried out a simple test simulation, with no star formation or outflows. In this simulation, as well as in the more detailed simulations described below, we fix the cosmological parameters to correspond to the observationally favored ΛCDM cosmology. In this case the current nonrelativistic matter, vacuum, and baryonic densities in units of the critical density are $\Omega_M = 0.35$, $\Omega_\Lambda = 0.65$, and $\Omega_b = 0.06$, while the Hubble constant, amplitude of mass fluctuations on the 8 Mpc h^{-1} scale, and cold dark matter "shape parameter" are taken to be $H_0 = 100\ h = 65$ km s^{-1} Mpc^{-1}, $\sigma_8 = 0.87$, and $\Gamma = 0.18$.

In the top panel of Figure 1, we compare the number density of collapsed dark matter halos as identified by a friends-of-friends group-finding algorithm with a linking length of $500^{-1/3}$ of the average interparticle spacing to the number density of halos as predicted analytically from a Press-Schechter approach. In the numerical case, the mass has been shifted by a factor of $\Omega_M/(\Omega_M - \Omega_b)$ to account for the fact that the analytical expression accounts for the total dark matter plus baryonic mass of the object. Here we see that while there is some discrepancy at the largest mass scales due to small-number statistics, this method of identification does well at all redshifts.

In the lower panel, we compare the number of dark matter halos with galaxies as identified from the distribution of the gas. Again the masses have been shifted by a factor of $\Omega_M/(\Omega_M - \Omega_b)$ in the dark matter case and by Ω_M/Ω_b in the case of the gas. Because of the increased condensation of gas relative to dark matter due to radiative cooling, a friends-of-friends linking length that is half that of the dark matter is necessary to give good agreement for all but the smallest mass scales. In this figure we also show the number density of galaxies as identified by the density-cut method described above, with two threshold values of $\delta_c = 200$ and $\delta_c = 500$. Again, both these values give reasonable agreement with the friends-of-friends dark matter and friends-of-friends gas particle identification schemes over a large range of mass scales. The identification of objects is quite dependent on this threshold on the lowest mass scales however, with the $\delta_c = 200$ case slightly overpredicting the number of objects relative to the dark matter friends-of-friends case, while the $\delta_c = 500$ cut gives slightly fewer low-mass objects than a friends-of-friends identification in the gas. In order to be conservative in the number of outflows

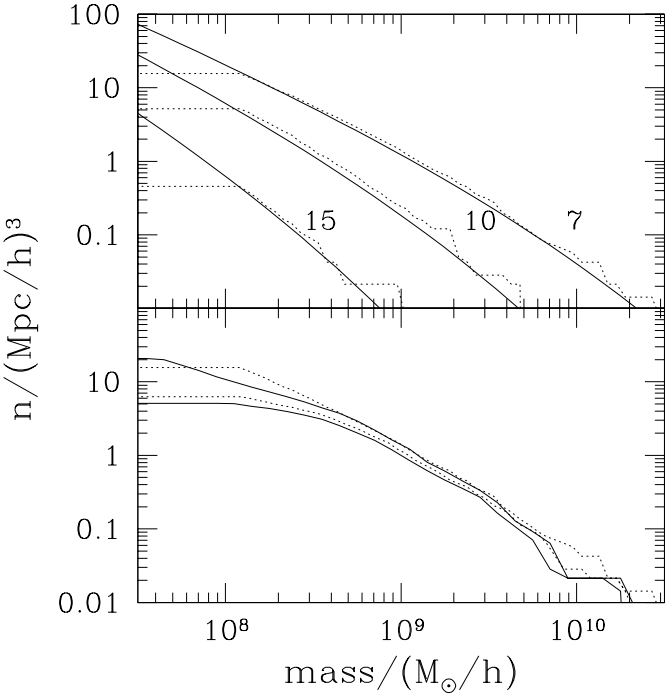

FIG. 1.—Identification of galaxies. *Top*: The number density of dark matter halos predicted by Press-Schechter theory (*solid lines*) and the number density identified by the friends-of-friends group finding algorithm (*dotted lines*) at three different redshifts. *Bottom*: The upper and lower dotted lines show the friends-of-friends number density of dark-matter halos with a linking length of $500^{-1/3}$ of the interparticle spacing and baryonic clouds with a linking length of $4000^{-1/3}$ of the interparticle spacing, respectively. The solid curves show the number density of galaxies as identified by a density cutoff of 200 (upper) and 500 (lower).

included in our simulations, as well as reproduce as closely as possible the results of a friends-of-friends identification of regions of virialized gas, we therefore adopt the higher density cut in our main simulations.

2.3. *Formation and Propagation of Galaxy Outflows*

Having developed a means of quickly identifying newly formed dwarf galaxies, we must also implement a model for star formation and outflows in these objects. For our model of star formation, we assume a simplified picture in which a fraction $\epsilon_{\rm sf}$ of the gas in a collapsed object is converted into stars in a single, initial burst of star formation. As all subsequent starbursts within a galaxy are likely to be much smaller and less efficient at generating outflows, this can be thought of as a conservative lower limit on the number of outflows formed.

In order to avoid multiple identifications of the same galaxy at each time step, and hence excessive star formation, we tag all particles that have previously been identified as part of a galaxy. Star formation is only implemented in cases in which over one-third of the galaxy, and at least 52 particles are untagged material that has not been previously considered as part of a collapsed object. Finally, in order to avoid excessively large outflows, we impose an upper limit of 1000 gas particles, corresponding to $5 \times 10^8\ M_\odot$ of gas that can be converted into stars in any one starburst.

As we are interested only in the number and spatial distribution of galaxies and are not attempting to reproduce their properties in detail, we simply take these stars to be formed out of the inner $\epsilon_{\rm sf}$ fraction of the gas particles, located closest to the center of mass. Apart from being easy to implement, this prescription also helps to delay excessive slowing down of the simulation as it reduces the net number of SPH neighbors in the densest regions.

Construction of outflows from these starbursting galaxies is likewise carried out in a simple manner, although in this case a slightly more sophisticated approach is necessary in order to properly reproduce outflows with realistic properties. The structure of outflows has been studied in detail by Mac Low & Ferrara (1999) and Ferrara & Tolstoy (2000), who conclude that efficient ejection of the interstellar medium or "blow-away" in disk galaxies occurs only in objects associated with halos with masses $\lesssim 10^7\ M_\odot$). In larger disks within halos in the mass range $10^7\ M_\odot \lesssim M \lesssim 10^9\ M_\odot$, a "blow-out" occurs in which the superbubbles around groups of Type II supernovae punch out of the galaxy, expanding freely perpendicular to the disk and shocking the surrounding IGM while failing to excavate the interstellar medium of the galaxy as a whole (see also Martel & Shapiro 2001). This scenario goes far in reconciling observations of expanding shells around dwarf galaxies (see, e.g., Axon & Taylor 1978; Marlowe et al. 1995; Heckman 1997; Martin 1998) and spectroscopy of high-z galaxies (Frye & Broadhurst 1998; Pettini 2001) with observations of multiple episodes of star formation in dwarf spheroidal galaxies (Smecker-Hane et al. 1994; Grebel 1998) some of which even suggest that many of these objects are gas rich, but with extended H I envelopes (Blitz & Robishaw 2000).

Guided by this blow-out scenario, we model the subresolution physics of outflow generation by rearranging the IGM surrounding an object into a galaxy superwind while leaving the central object intact. We construct our outflows from all gas particles with $r_N < r < r_O$, where r_O is the maximum of twice the radius of the object identified as a galaxy and the radius within which 104 additional particles are located ($r_O = \max\,[2r_N, r_{N+104}]$). All the objects within the galaxy radius, r_N, on the other hand, are left unchanged apart from the simple conversion of a fixed fraction of gas particles to stars. These outflow particles are then arranged on two concentric spherical shells of radius r_O and $0.9r_O$. This multishell structure assures that the outflows will be sufficiently well-resolved radially to be reasonably treated by the SPH solver. Sufficient resolution along each of the shells is assured by arranging the particles in each of the shells to be anticorrelated such that no two particles are within a distance of less than one-half of the average spacing between neighbors. This minimizes the subrandom particle distribution that arises naturally within SPH. The particles in both shells are then given velocities

$$\boldsymbol{v}_{i,\rm shell} = \boldsymbol{v}_{\rm cm} + \hat{\boldsymbol{r}}_{\boldsymbol{i}}\, v_{\rm rad} + \boldsymbol{v}_{\boldsymbol{i}\rm ang}\,, \tag{6}$$

where $\boldsymbol{v}_{\rm cm}$ is the center of mass velocity of the galaxy, $v_{\rm rad}$ is a boost in the radial direction due to the outflow, and $\boldsymbol{v}_{\boldsymbol{i}\rm ang}$ is an axial velocity necessary to conserve angular momentum.

Just as we have assumed in all cases that a fixed fraction of the gas in the object, $\epsilon_{\rm sf}$, forms stars, we now assume that a fixed fraction of the energy from the resulting supernovae, $\epsilon_{\rm wind}$, is channeled into the outflow. Following the prescriptions adopted in SB we estimate that one supernova occurs for every $100\ M_\odot$ that form stars (see, e.g., Gibson 1997) and that each of the supernovae has a kinetic energy of output of 2×10^{51} ergs, to take into account the contribution from stellar winds. The radial velocity of the shell is then taken

such that $1/2N_{\rm shell} m_g v_{\rm rad}^2 = {\rm KE} - {\rm PE}$, where $N_{\rm shell}$ is the number of particles used to construct the outflow, KE is the kinetic energy channeled into the outflows, and PE is the potential energy to move the particles from their original locations to the two concentric shells. Approximating the total mass of the galaxy as $Nm_g\Omega_M/\Omega_b$, this gives

$$v_{\rm rad} = 200 \text{ km s}^{-1}\left(\frac{N}{N_{\rm shell}}\right)^{1/2}\left(\frac{\epsilon_{\rm sf}}{0.1}\frac{\epsilon_{\rm wind}}{0.1} - 2.1\times10^{-10}\right) \times\left[\frac{m_g}{M_\odot}\frac{\Omega_M}{\Omega_b}\left(\sum_{i=N+1}^{N+N_{\rm shell}}\frac{1\text{ kpc}}{r_i} - \frac{1\text{ kpc}}{r_O}\right)\right]^{1/2}. \quad (7)$$

Note that this method relies on an unsoftened potential-energy estimate so that the shell does not have an excess of kinetic energy as would result from a softened potential-energy approach. Finally, to compute $\boldsymbol{v}_{i\rm ang}$ we take the angular momentum vector of the particles used to construct the outflow about the center of mass and apply a solid body rotation to the shell in the same direction and with the same magnitude:

$$\boldsymbol{v}_{i\rm ang} = \frac{\boldsymbol{L}\times\boldsymbol{r}_{i\rm shell}}{(r_O)^2 N_{\rm shell}}, \quad (8)$$

where $\boldsymbol{L} = \sum_{i=N+1}^{N+N_{\rm shell}} \boldsymbol{r}_i \times \boldsymbol{v}_i$.

In order to compare this outflow scheme with analytical estimates, we have carried out a test simulation in which we fix $\epsilon_{\rm sf} = \epsilon_{\rm wind} = 0.1$ and study the collapse and outflow evolution of a spherical overdensity. In a 1.8 Mpc cubic comoving region containing 2×50^3 particles, we arranged the matter within a 300 kpc radius into a spherical "top hat" overdensity, such that it would collapse and virialize at a redshift of two. For simplicity we considered an Einstein–de Sitter cosmology in which $\Omega_M = 1$, $\Omega_\Lambda = 0$, $\Omega_b = 0.06$, and $h = 0.5$. With these parameters, the top hat contained approximately 2469 gas and dark matter particles of masses 2.1×10^6 and 1.3×10^5 $M_\odot$, respectively, resulting in a total mass of 8.5×10^9 $M_\odot$. While the original baryonic mass of this perturbation was 4.5×10^8 $M_\odot$, only approximately half of this mass collapsed into the final galaxy, due to the reduction in accreted gas caused by the expanding shell. This effect was also observed in our larger simulations and is discussed in more detail below.

The trajectory of the outflow is shown as the dashed lines in Figure 2. At each time we calculated the velocity and radius in the radial bin that contained the highest momentum. The sharp change in the radius at 0.5 Gyr is due to the presence of an extremely low-density gap left behind after the top hat collapses. When the shock moves into this region, the low-density gas is heated and accelerated to velocities greater than that of the dense material, while conserving overall radial momentum. As a result the material spreads out and the peak becomes less defined, shifting from the center to near the front of the shock. This jump is particularly clear when contrasted with the dotted lines, which show the analytical solution taken from SB for a model with $\epsilon_{\rm sf} = \epsilon_{\rm wind} = 0.1$ and an object with a total mass of 8.5×10^9 $M_\odot$. Here the shock is modeled as a thin spherical shell of material which is accelerated due to internal pressure and escapes from the gravitational pull of the halo into the Hubble flow. Note that although the SB model also takes into account the Compton drag due to the scattering of electrons against CMB photons, this contribution is negligible at $z = 2$.

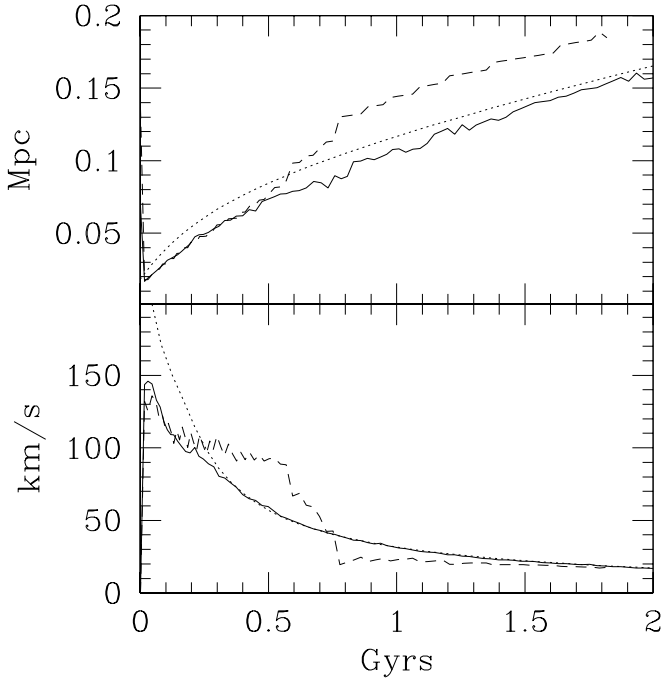

FIG. 2.—Comparison between SPH simulations and analytical modeling. The solid lines and dashed lines correspond to outflows from the top-hat within the Hubble flow and pure top-hat simulations, respectively, as discussed in § 2.3; while the dotted lines correspond to the thin-shell model adopted in SB. In all cases the overdense region is a 300 comoving kpc sphere that collapses at $z = 2$ in an Einstein–de Sitter cosmology. The time derivative of the radius in the pure top hat does not correspond to the velocity as the peak bin shifts in this simulation as the shock passes through the empty region.

While the high velocities in the analytical solution at early times ($\leq$0.2 Gyr) are due to the pressure driven nature of the early outflow solution, the discrepancies at later times are clearly a relic of the existence of the unnatural empty region in the SPH simulation. In order to be able to more directly compare our simulations to the thin shell model then, we conducted a final test in which we excised the central collapsed object and early outflow from this empty region and superimposed it on a uniform 1.8 Mpc cubic box of particles expanding with the Hubble flow. The results of this simulation are shown as the solid lines, for which the velocities agree almost exactly for all times after the early pressure-driven phase. Note also that the early shell velocities in all of these models are consistent with those observed in Lyman break galaxies at similar optical radii (Pettini 2001).

3. RESULTS AND DISCUSSION

In order to evaluate the impact of galaxy outflows on structure formation, we have conducted two simulations: a main outflow run with $\epsilon_{\rm sf} = 0.1$ and $\epsilon_{\rm wind} = 0.1$ corresponding to the fiducial model examined in SB, and a comparison "no-outflows case" in which star formation is implemented with the same efficiency, but no outflow particle rearrangements and velocity boosts are implemented. Our philosophy is not to attempt to refine these parameters in order to best reproduce the observed properties of dwarf galaxies, but rather to study the qualitative features that arise in a simple, conservative model of galaxy outflows. Once the SPH particles in a given region reach their minimum allowed smoothing length, further clustering causes the

number of SPH neighbor particles to rise without limit. Although the transfer of gas to stars helps to alleviate the subsequent algorithmic slow-down, the N^2 nature of clustered regions leads to a significant load imbalance in the parallel code. Hence, we limited the evolution of the simulations to $z = 6$, which is more than sufficient to detail the properties of the dwarf galaxy distribution under the influence of outflows. Evolution to this epoch required over 2000 steps, with a minimum time step of 0.4 Myr. Notably, the run with outflows required 5% fewer time steps because dense regions, which usually dictate the shortest time steps, form with less efficiency. Each simulation required approximately 10 days of computing time on a 16 node Sun E6500 server.

3.1. *Global Properties and Observational Checks*

In Figure 3 we plot the distribution of outflows as a function of initial velocity. While the lower peak in this plot is almost certainly a relic of the minimum mass scale at which we identify objects as galaxies, a large fraction of the winds are generated with significantly higher initial velocities. All velocities are consistent with observations of high-redshift dwarf galaxies (Frye & Broadhurst 1998; Warren et al. 1998; Pettini 2001).

In the top panel of Figure 4 we show the overall star formation rates (SFRs) in these simulations. While these rates are equivalent at extremely early times, almost immediately the addition of outflows to the simulation greatly reduces the mass of gas passing the density-cut criteria, reducing the SFRs in the outflow simulation by a factor of approximately 3. For comparison, we also show on this plot the SFR as calculated in the semianalytical model described in SB. Here star formation occurs at slightly higher redshifts, due to the stringent density-cut criteria chosen to identify galaxies in our simulations. At late times, however, both these rates become roughly similar. These values are also roughly consistent with measurements at redshifts 3 and 4 and extrapolations to the redshift range in our simulation (see, e.g., Steidel et al. 1999; Percival, Miller, & Ballinger 1999; Gallego et al. 1995).

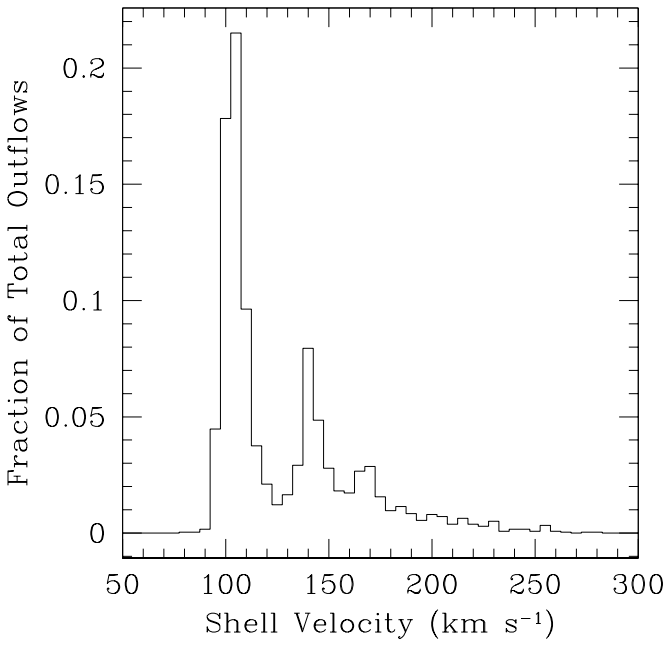

FIG. 3.—Histogram of outflows as a function of initial shell velocity. The lower 100 km s^{-1} peak is a relic of the minimum galaxy mass in the simulation. There are 2367 outflows in the (5.2 Mpc h^{-1})^3 comoving volume by a redshift of 6.

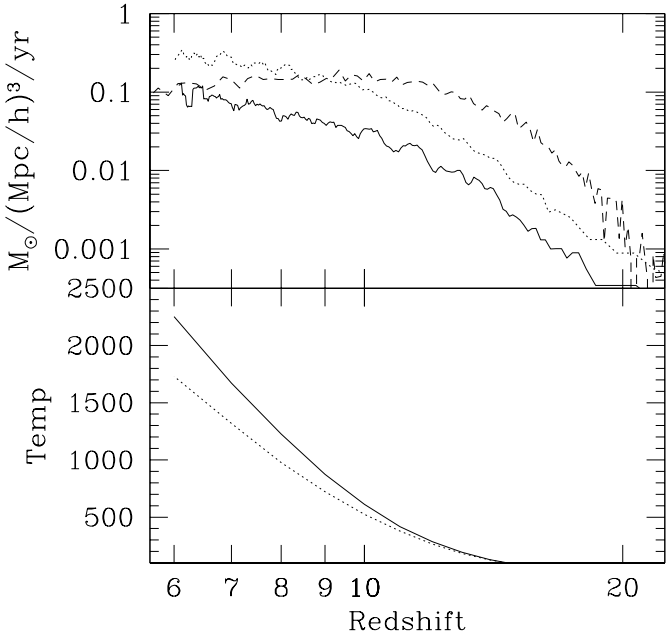

FIG. 4.—*Top:* Global star formation rate. The star formation rate in the outflows simulation is given by the solid line, while the star formation only simulation is represented by the dotted line. For comparison, the dashed line shows the semianalytical star formation rate calculated in SB for the fiducial outflows model. *Bottom:* Mean temperature of the gas in the outflow (*solid line*) and star formation only (*dotted line*) simulations.

Finally, in the lower panel of this figure, we show the average temperature of the gas particles in the simulation. Here we see that outflows have only a secondary impact, the majority of gas heating being the result of energy released by gravitational collapse and virialization. Nevertheless, the overall increase in IGM temperature pushes our model in a direction that is favorable to X-ray background considerations (Pen 1999), and the overall degree of heating is well within other observational limits. A main probe of this heating is the degree of spectral distortions in the Cosmic Microwave Background, due to scattering of microwave photons off the hot ionized gas. The magnitude of these distortions is given by the Compton-y parameter which is the convolution of the optical depth with the electron temperature along the line of sight (see, e.g., Zel'dovich & Sunyaev 1969; Sunyaev & Zel'dovich 1972). In our models the contribution to this effect from redshifts above 6 is $y = 1.1 \times 10^{-7}$ in the outflows case and $y = 1.0 \times 10^{-7}$ in the star formation only case. These values are much less than the observational constraint of $y \leq 1.5 \times 10^{-5}$ (Fixsen et al. 1996).

3.2. *Suppression of Dwarf Galaxy Formation and Baryonic Stripping*

The great reduction in star formation in the outflows case is indicative of a large difference in the total mass in galaxies between the two runs. In order to understand how this difference is distributed over the range of galaxy masses, in Figure 5 we compare the number densities of galaxies in both runs at a number of redshifts. Again, we use the density-cut method of identifying objects with a threshold

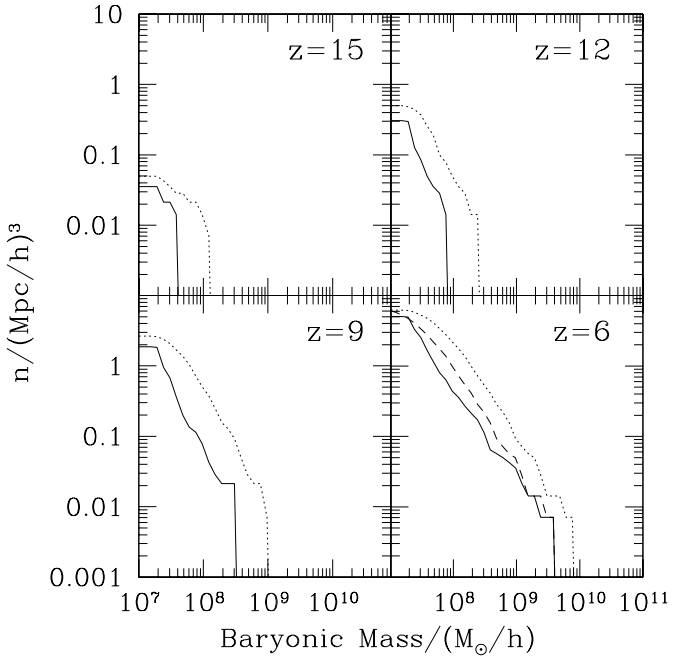

FIG. 5.—Number density of galaxies, now in terms of baryonic mass. In each panel the solid lines are from the simulation with galaxy outflows, and the dotted lines are from the star formation only simulation. Notice that there is both an overall offset in mass between the two runs, as well as an additional suppression of halos on the $\sim 10^8\ M_\odot \approx 10^9\ M_\odot\ \Omega_b/\Omega_0$ scale. For comparison, the dashed line at $z = 6$ shows the no-outflows run shifted in mass by a factor of 2.

value of $\delta_c = 500$, and shift the total gas mass by a factor of Ω_M/Ω_b to approximate the total mass of the object.

Here we see that outflows have two major effects on the distribution of objects. First, as in the test case discussed in § 2.3, they somewhat restrict the amount of gas that each object can accrete, shifting the number distribution to smaller masses at all mass scales. Thus, while galaxies in the $\sim 10^7$ to $\sim 10^{10}\ M_\odot$ range may have been unable to eject large fractions of their own interstellar medium, the strong winds of IGM material they are able to "blow out" at early times greatly reduce the amount of gas they accrete over their lifetimes. This is similar to the mechanism described by Dekel & Silk (1986) in which high dark matter fractions are caused by supernova-driven winds from high-mass stars formed early in the history of a dwarf galaxy, resulting in a systematic bias toward higher mass-to-light ratios.

In addition to this mass shift, Figure 5 shows a large deficit in the overall number of objects with masses below $5 \times 10^9\ M_\odot$. At $z = 6$ for example, even when accounting for a $\sim 50\%$ shift in masses between the two runs, there are less than half the number of galaxies in this range in the outflows simulation than in the no-outflows case. This difference is extremely suggestive of the "baryonic stripping" mechanism identified in our previous studies, in which outflows from early galaxies remove the gas from nearby overdense regions that would have otherwise later formed into dwarf galaxies. In these regions, the gas is stripped away from the collapsing dark matter and ejected into space along with the outflow, leaving behind only an empty "dark halo" of nonbaryonic matter. In SB, baryonic stripping reduced the number of $\sim 10^9\ M_\odot$ objects by $\sim 75\%$.

In order to study this mechanism further in our SPH simulations, we have selected two 60^3 kpc^3 physical (420^3 kpc^3 comoving) regions at a redshift of 6: one a typical region of galaxy formation, and the second a more extreme example with higher velocity outflows. These regions have been extracted from both simulations and used to construct contour plots of total gas mass projected in the z-direction, shown in Figure 6.

In this figure we can see both the reduction of gas accretion in outflowing dwarfs, and the baryonic stripping of neighboring objects. The typical galaxy-forming region shown in the upper two panels emphasizes the first of these two mechanisms. While both runs contain the same number of dense peaks in the gas distribution, these are somewhat larger and more concentrated in the no-outflows case. Thus, the two largest peaks in the center of the volume have much the same positions and central mass profiles in both cases, while much of the mass on the outer edges has been ejected into a large cloud rather than accreted by the galaxies themselves. Note also that no outflows occurred in the less dense regions such as that near the bottom of these panels, and thus the distribution of matter in this area is completely equivalent between the two runs.

In the extreme outflow regions shown in the bottom two panels of Figure 6, reduced accretion is again visible, but now complemented by several examples of baryonic stripping. Notice, for example, that the two smaller mass peaks to the left of the central object in these panels have been almost completely disrupted by the spherical wind emanating from this object. Notice also that this mechanism is extremely sensitive to the relative formation times between objects. Thus, while the two peaks directly above and to the right of the central object are of similar sizes in the star formation only run, the outflow from the first of these objects to form has completely suppressed the other's formation in the outflows run. A careful inspection of these panels uncovers several other examples of baryonic stripping and slowing of accretion, although again, the lowest density regions are completely equivalent.

In order to further quantify this suppression of objects, we make use of the fact that while outflows greatly affect the number and distribution of galaxies, their effect on the sizes and positions of collapsed dark matter halos is only of secondary importance. Using the friends-of-friends group finder method with a linking length of $500^{-1/3}$ of the average interparticle spacing, we have computed lists of dark matter halos as described in § 2.2. For each of these objects we identify a center-of-mass position along with an average distance from the center of mass to the particles in the halo, R_A. We then calculate the mass of galaxies lying within each halo by tagging all "galaxies," as defined by our density cut criteria, whose center of mass lies within fR_A, where f is some fraction. Here we fix $f = 2.0$, although varying this quantity from 1.5 to 2.5 has little effect on our results.

In the upper panel of Figure 7 we plot the number of halos as a function of halo mass that contain at least one galaxy as defined in § 2.2. Here we see that the no-outflows run has a significantly larger population of halos in the $\sim 10^9\ M_\odot$ range that contain galaxies. Note that this deficit cannot be caused simply by a reduction of accretion, as this histogram contains all halos that host a galaxy of any size.

This difference can also not be attributed simply to a difference in the number of dark matter halos in both simulations. In the lower panel of Figure 7 we have correlated the halos between the simulations, requiring that their

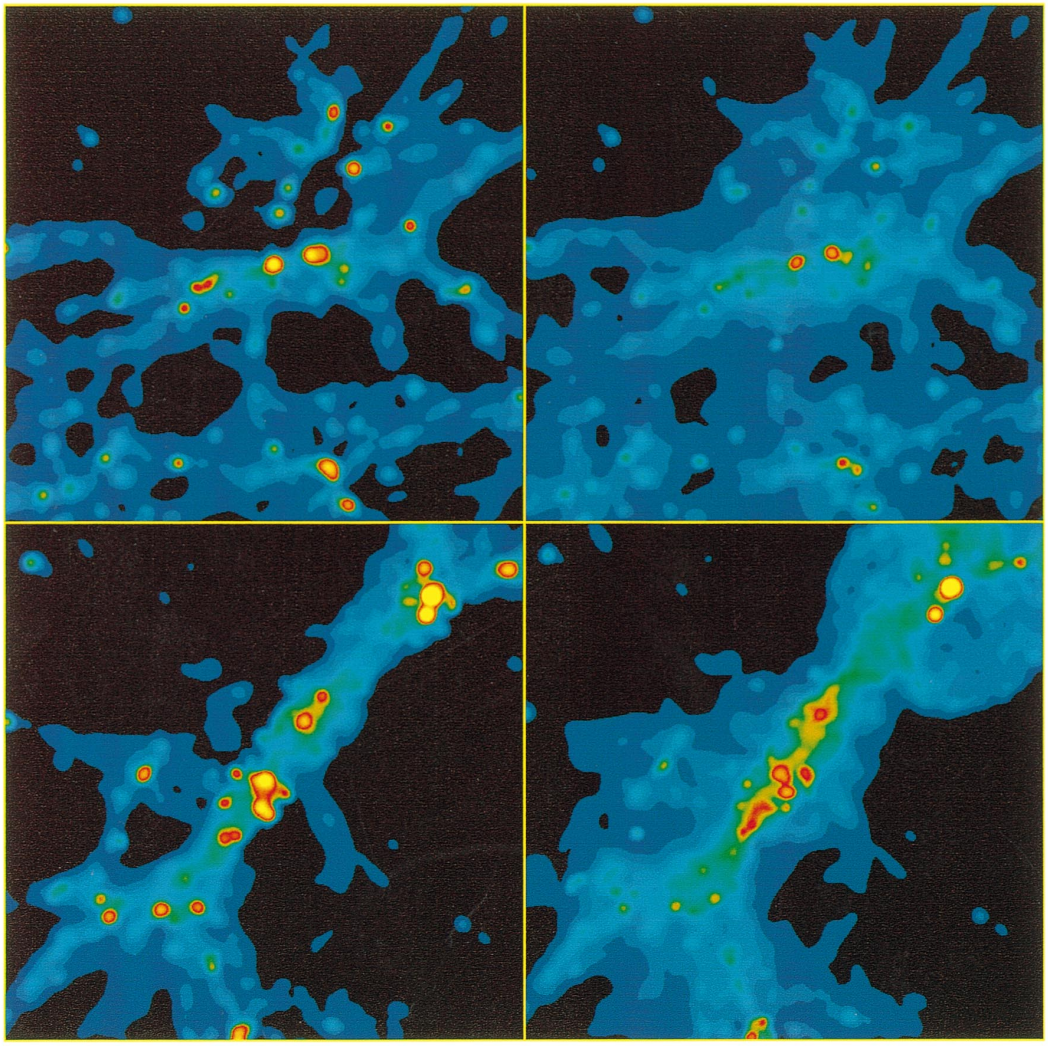

FIG. 6.—Mass contours of two 80^3 kpc^3 physical (560^3 kpc^3 comoving) regions from each of the simulations at a redshift of 6. The colors are arranged in equal contours from $1.3 \times 10^{10}\ M_\odot$ to $6.5 \times 10^{11}\ M_\odot$/(comoving Mpc)^2, while the mean density in this cosmology is $9.3 \times 10^9\ M_\odot$/(comoving Mpc)^2. The upper two panels show a typical region of galaxy formation. In the lower two panels, we look at a vigorous galaxy formation. In each pair, the left panel is taken from the no-outflows run, while right panel is from the run with galaxy outflows.

centers of mass be located within 1 kpc of each other. In this case we show the number of correlated halos with a galaxy in the outflows simulation, compared the correlated halos with galaxies in both simulations. While the overall number of halos is reduced slightly due to small differences in the halo distribution, we see again that a large number of the filled halos in the no-outflows case are empty in the corresponding outflows run. Finally, we compute the number of halos that contain a galaxy in the no-outflows run, but contain less than a quarter of that mass in galaxies in the outflow case. These examples of severe suppression persist up to the $10^{10}\ M_\odot$ scale.

Finally, we chose a typical halo that is empty in the fiducial case and filled in the no-outflows run and study its history in greater detail. In Figure 8 we plot the total dark and gas matter masses within the object itself, defined as the mass within a 10 comoving kpc h^{-1} sphere centered around the center of mass of a dark matter halo with a mass of 5×10^8 a redshift of 6. We then compare the evolution of this mass to the star formation rate within a fixed 6.5 kpc h^{-1} sphere representing the object's immediate environment. At early times, the evolution of the object is the same in both runs, until the initial burst of nearby star formation at a redshift of 9. As the outflow corresponding to this burst sweeps though the halo, the total number of baryons diverges between the two runs, while the number of dark matter particles remains almost the same. By a redshift of 6, the no-outflows object has accreted almost twice the gas of the object in the outflow run. Note that this discrepancy is of a different nature than the mass shift described in § 2.3 as it is caused by environmental effects rather than winds emanating from the object itself. Indeed, no star formation occurs at any redshift ≥ 6 in the object in the fiducial run, and only the no-outflows object passes the density cut to be considered a galaxy and forms stars. Notice also that while environmental effects are able to suppress this object only in the outflows case, the total degree of environmental star formation is actually much greater in the no-outflows simulation, as neighboring objects accrete gas more easily in this model.

3.3. *Theoretical Uncertainties*

While the simple "blow-out" scenario we have studied strives to illustrate the qualitative effects of dwarf outflows

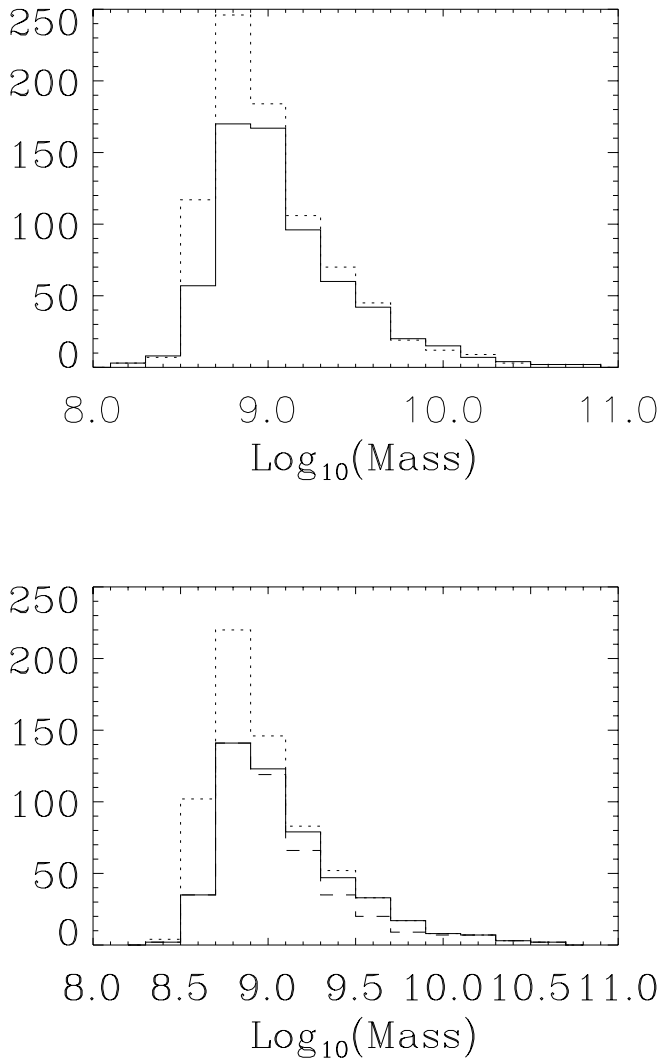

FIG. 7.—Baryonic stripping and empty halos. *Top:* Histograms of dark matter halos that contain at least one condensed galaxy. The solid lines correspond to the outflows run and the dotted lines to the star formation only case. *Bottom:* Histograms of dark halos that have been correlated between the two runs. The dotted line shows all correlated halos that contain a galaxy in the star formation only run and the solid line shows all halos with galaxies in both simulations. Finally, the dashed line shows all halos with galaxies in the star formation only run, and galaxies with at least 1/4 of that mass in the outflows run.

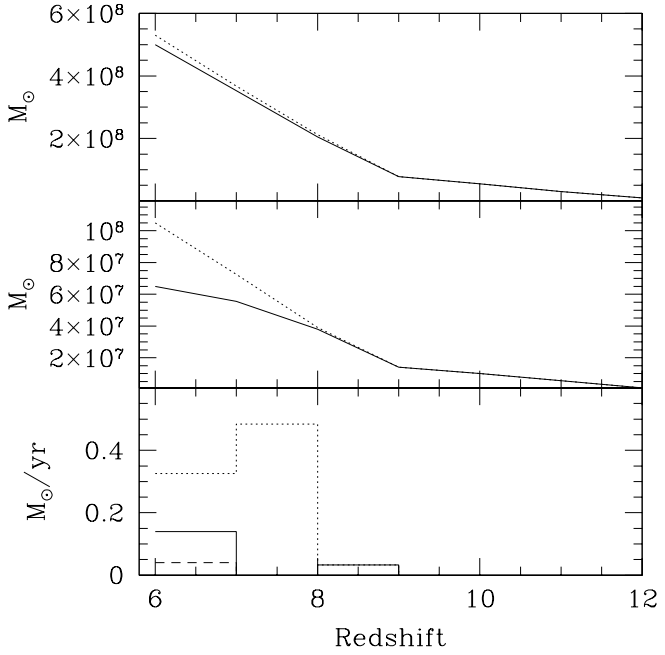

FIG. 8.—Baryonic stripping in a typical halo. The upper and center panels show the total dark matter and baryonic mass, respectively, within a 10 kpc h^{-1} comoving sphere centered around a halo that experiences baryonic stripping. The solid lines correspond to the fiducial outflows run, while the dotted lines are taken from the run with no outflows. In the lower panel the solid and dotted lines show the star formation rate in the 6.5 physical kpc h^{-1} sphere representing the environment of the halo in the no-outflow and fiducial runs, respectively, while the dashed line shows the star formation rate within the 10 kpc h^{-1} object itself in the no-outflows case. The are no stars formed with the object itself in the fiducial run.

on structure formation, without attempting to reproduce the process in detail, it nevertheless contains a number of free parameters that deserve some scrutiny. The most important and uncertain of these values for our simulations is the product of $\epsilon_{\rm sf}$ and $\epsilon_{\rm wind}$, which compounds the uncertainty in starburst size with the uncertainty in the fraction of that energy that is channeled into the winds. The star formation efficiency is one of the most complicated and notoriously uncertain parameters in all of astrophysics, and as such there is little we can do to definitively fix this number. Our value is thus simply chosen to be somewhat middle of the road among estimates (e.g., Tegmark, Silk, & Evrard 1993; Majumdar, Nath, & Chiba 2000) and consistent with observed SF rates at high redshift.

Similarly, $\epsilon_{\rm wind}$ is largely uncertain and is chosen to be a somewhat conservative value, consistent with previous estimates (e.g., Heckman, Armus, & Miley 1990; Scannapieco & Broadhurst 2001; Madau et al. 2000). Note that our choice of $\epsilon_{\rm sf}\,\epsilon_{\rm wind} = 0.01$ results in outflow velocities that are consistent with and even smaller than those observed and does not cause excessive heating of the IGM beyond Compton constraints, and thus we can have some confidence that this is a reasonable value to consider. Our goal, after all, is not to present a definitive model of galaxy outflows, but rather an illustrative example of the role that they play at high redshift: a picture that will undoubtedly be refined as our theoretical and observational understanding of galaxy outflows progresses.

While these uncertainties are unavoidable in any study of high-redshift outflows, our model also contains an additional parameter that is specific to how burst-mode star formation is implemented. Since accretion occurs over a number of time steps it is difficult to ascertain when an object has accumulated enough material to be considered a "new galaxy," and thus to undergo a starburst. In our fiducial and no-outflow models we implemented a "one-third" rule, adding a starburst whenever a fraction $f_B = 1/3$ or 52 particles in a galaxy were new material. The 1/3 value was initially chosen as it corresponds to a similar threshold used in the semianalytic model developed in SB. Setting $f_B = 0$ would result in each galaxy undergoing a new starburst with each small amount of gas accreted, constantly creating new stars and rearranging the surrounding IGM material into outflows. Adopting a very high value would likewise result in an equally unphysical situation in which galaxies were forced to remain quiescent for a long latency period,

accreting huge amounts of gas before they finally explode in massive outflows.

In order to be certain that our simulations lie somewhere between these unphysical extremes, we have carried out a number of tests runs in a periodic comoving box of size 3.0 h^{-1} Mpc with 2×96^3 particles. The mass resolution in this case is $3.9 \times 10^6\ M_\odot$ for the dark matter and $7.8 \times 10^5\ M_\odot$ for the gas. We again fixed $\epsilon_{sf} = 0.1$ and made four different outflow runs with $\epsilon_{wind} = 0.1$, one with no lower limit on the fraction of new particles necessary to be considered a new galaxy, and three runs where we allowed f_B to vary between 1/4, 1/3, and 1/2. Finally, we conducted a comparison no-outflows test run with $\epsilon_{wind} = 0$.

The resulting number distributions appear in Figure 9. Here we see that while changing f_B does introduce some uncertainty in the number of objects formed in the outflow simulations, these uncertainties are small in comparison with the difference between these runs and the no-outflows case. Furthermore, at all masses, the number of objects increases monotonically with increasing threshold, thus demonstrating that even at a somewhat high value of $f_B = 1/2$, unphysically powerful superwinds do not conspire to increase or bias the impact of galaxy outflows from the behavior seen in the less-punctuated models. Relaxing the threshold entirely, on the other hand, results in a huge reduction in the amount of gas accreted by the galaxies, as outflows and IGM rearrangements are implemented every few times steps. A simple visual inspection of this run confirmed that the majority of the galaxies in the volume were little more than groupings of star particles, surrounded by concentric spherical shells. Based on these results, we can have some confidence that by adopting an intermediate threshold value of 1/3, our simple model is able to reproduce the qualitative features of the impact of galaxy outflows on the formation of dwarf galaxies.

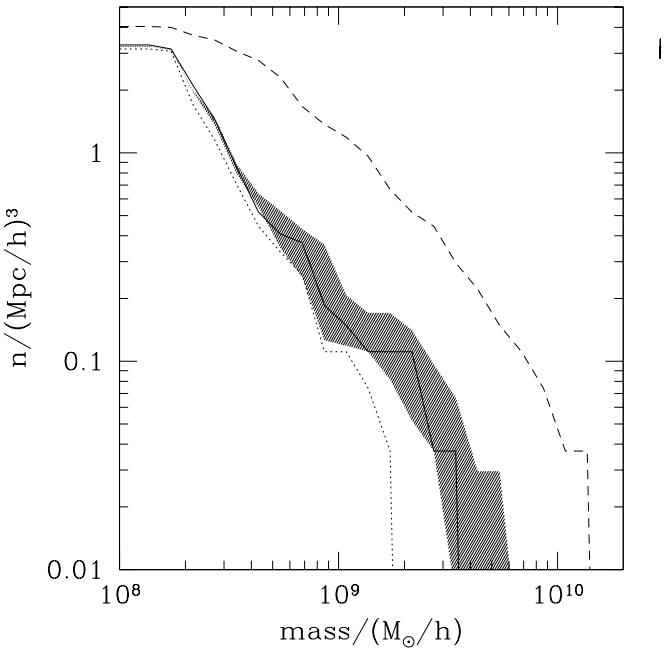

FIG. 9.—Number density of galaxies in the various comparison runs at a redshift of 6. The solid line is from the outflow simulation with $f_B = 1/3$ and the shaded region is bounded by the results of varying f_B from 1/4 to 1/2. The dotted line represents an outflow simulation in which $f_B = 0$, while the dashed line shows the results of the test run with no outflows. Although varying the threshold value introduces some uncertainty in the number of objects in the outflow runs, these changes are small when compared with the no-outflows case.

Finally, the spherical model adopted in our simulations is unquestionably oversimplified, as observed outflows such as those in M82 (e.g., Shopbell & Bland-Hawthorn 1998) eject matter preferentially along the spin axis of the galaxy. Adopting a collimated model would result in slightly larger accretion rates, as matter would be able to more easily fall onto the galaxies along the plane of the disk. In such a model, the mass shift in Figure 5 would be reduced, dependent on the unknown beaming angle. Galaxy suppression by baryonic stripping, on the other hand, is likely to change little in such a model, as the spin axes of galaxies are only weakly correlated with large-scale structure, and furthermore only poorly resolved for the smaller galaxies in our simulations.

4. CONCLUSIONS

Despite the overwhelming observational evidence for galaxy outflows at high and low redshift, the impact of this process on galaxy formation has been little explored. While all numerical galaxy formation simulations carried out to date assume formation in primordial conditions, exploratory semianalytical studies have suggested that many galaxies form under much different circumstances.

In this work, we have implemented a simple "blow-out" model for feedback from supernova generated winds, to study the impact of outflows on the formation of high-redshift dwarf galaxies in a characteristic volume of the universe. While these simulations avoid galaxy self-annihilation or "blow-away" by construction, they have uncovered two major mechanism by which outflows impact the formation of dwarf galaxies.

First, outflowing dwarf galaxies impact their own formation by slowing down the further accretion of gas. This causes an overall decrease of about 50% in the total gas mass accreted by these objects which is roughly constant over the mass range studied in our simulations.

In addition to this mechanism, and perhaps more interestingly, our SPH simulations have also uncovered a significant number of would-be dwarves whose formation has been suppressed by baryonic stripping by neighboring objects. In these cases, the winds from nearby objects reach the overdense region sufficiently early to eject the gas from the collapsing dark matter perturbation. This results in a large fraction of $\sim 10^9\ M_\odot$ empty halos in which the dark matter has virialized but no baryonic gas has collapsed.

While our simulations are only able to identify this suppression at high redshift, this mechanism is suggestive of the discrepancy between the number of observed Milky Way satellites and predictions from CDM models that do not include outflows (Klypin et al. 1999; Moore et al. 1999). The dark halos generated in this scheme also provide a natural explanation for the existence of massive yet extremely gas-poor extragalactic high-velocity clouds (see, e.g., Blitz et al. 1999), as well as the observed lack of low-mass galaxies in the field relative to dense clusters (e.g., Phillips et al. 1998). Note that as pointed out by Trentham, Möller, & Ramirez-Ruiz (2001) the existence of a large number of empty halos does not depend on the detailed predictions of the CDM model but follows simply from the assumption that the mass function of dark matter halos does not vary with environment, thus suggesting that the observed environ-

mentally dependent suppression of dwarf formation is due to astrophysical considerations rather than some unknown properties of the dark matter or the primordial power spectrum (e.g., Kamionkowski & Liddle 2000; Spergel & Steinhardt 2001).

Our results rely on a simple model of outflow formation in a limited volume of the universe at redshifts above 6, and thus can not be directly compared with observations. Nevertheless, the lesson to be drawn from these simulations is clear. Just as in the case of galaxy clusters, outflows profoundly affect the formation and distribution of dwarf galaxies. These effects are not confined simply to the properties of the outflowing galaxies themselves but the formation of objects nearby, and this interaction between neighbors plays an important role in the history of the formation of galaxies. While the assumption of primordial conditions is a good first step in the study of this problem then, we will never fully understand galaxy formation until we have first understood mechanical feedback from galaxy outflows.

We would like to thank Tom Broadhurst and Andrea Ferrara for helpful comments and discussions. E. S. has been supported in part by an NSF fellowship. This project was supported by NSF KDI grant 9872979.

REFERENCES

Axon, D. J., & Taylor, K. 1978, Nature, 274, 37
Benz, W. 1990, in Numerical Modeling of Nonlinear Stellar Pulsations: Problems & Prospects, ed. J. Robert (Dordrecht: Kluwer), 269
Blitz, L., & Robishaw, T. 2000, ApJ, 541, 675
Blitz, L., Spergel, D. N., Teuben, P. J., & Hartmann, D., & Burton, W. B. 1999, ApJ, 514, 81
Bomans, D. J., Chu, Y.-H., & Hopp, U. 1997, AJ, 113, 167
Bromley, B. C., Press, W. H., Lin, H., & Kirshner, R. P. 1998, ApJ, 505, 25
Bryan, G. L. 2000, ApJ, 540, L39
Cavaliere, A., Menci, N., & Tozzi, P. 1999, MNRAS, 415, 50
Ciardi, B., Ferrara, A., Governato, F., & Jenkins, A. 2000, MNRAS, 314, 611
Couchman, H. M. P. 1991, ApJ, 386, L23
Couchman, H. M. P., Thomas, P. A., & Pearce, F. R. 1995, ApJ, 452, 797
Davis, M., Efstathiou, G., Frenk, C. S., & White, S. D. M. 1985, ApJS, 57, 241
Dekel, A., & Silk, J. 1986, ApJ, 303, 39
della Ceca, R., Griffiths, R. E., Heckman, T. M., & MacKenty, J. W. 1996, ApJ, 469, 662
Eke, V. R., Navarro, J. F., & Frenk, C. S. 1998, ApJ, 503, 569
Ferrara, A., & Tolstoy, E. 2000, MNRAS, 313, 291
Fixsen, D. J., Cheng, E. S., Gales, J. M., Mather, J. C., Shaver R. A., & Wright, E. L. 1996, ApJ, 473, 576
Frye, B., & Broadhurst, T. 1998, ApJ, 499, L115
Gallego, J., Zamorano, J., Aragon-Salamanca, A., & Rego, M. 1995, ApJ, 445, L1
Gerritsen, J. P. E. 1997, Ph.D. thesis, Kapetyn Astron. Inst.
Gibson, B. K. 1997, MNRAS, 290, 471
Gingold, R. A., & Monaghan, J. J. 1977, MNRAS, 181, 375
Grebel, E. 1998, in IAU Symp. 192, The Stellar Content of Local Group Galaxies, ed. P. Whitelock & R. Cannon (San Francisco: ASP), 17
Haiman, Z., Rees, M., & Loeb, A. 1997, ApJ, 476, 458 (erratum 484, 985 [1997])
Heckman, T. 1997, Rev. Mexicana Astron. Astrof., 6, 156
Heckman, T., Armus, L., & Miley, G. K. 1990, ApJS, 74, 883
Hultman, J., & Pharasyn, A. 1999, A&A, 347, 769
Kaiser, N. 1991, ApJ, 383, 104
Kamionkowski, M., & Liddle, A. R. 2000, Phys. Rev. Lett., 84, 4525
Katz, N. 1992, ApJ, 391, 502
Klypin, A., Kravtsov, A. V., Valenzuela, O., & Prada, F. 1999, ApJ, 522, 82
Lacy, C., & Cole S. 1995, MNRAS, 271, 676
Lucy, L. B. 1977, AJ, 82, 1013
Mac Low, M. M., & Ferrara, A. 1999, ApJ, 513, 142
Madau, P., Ferrara, A., & Rees, M. J. 2000, ApJ, 555, 92
Majumar, S., Nath, B. B., & Chiba, M. 2001, MNRAS, 324, 537
Marlowe, A. T., Heckman, T. M., Wyse, R. F. G., & Schommer, R. 1995, ApJ, 438, 563
Martel, H., & Shapiro, P. R. 2001, Rev. Mexicana Astron. Astrofis. Ser. de Conf., in press
Martin, C. L. 1998, ApJ, 506, 22
Metzler, C. A., & Evrard, A. E. 1994, ApJ, 437, 564
Mihos, C., & Hernquist, L. 1994, ApJ, 437, 611
Moore, B., Ghinga, F., Governato, G., Lake, T., Quinn, T., Stadel, J., & Tozzi, P. 1999, ApJ, 524, L19
Mushotzky, R. F., & Scharf, C. A. 1997, ApJ, 482, L13
Nath, B., & Trentham, N. 1997, MNRAS, 291, 505
Navarro, J. F., & White, S. D. M. 1993, MNRAS, 265, 271
Pearce, T. J., Thomas, P. A., Couchman, H. M. P., & Edge A. C. 2000, MNRAS, 317, 1029
Pen, U.-L. 1999, ApJ, 510, L1
Percival, W., Miller, L., & Ballinger, B. 1999, in ASP Conf. Ser. 193, The Hy-Redshift Universe: Galaxy Formation at High Redshift, ed. A. J. Bunker & W. J. M. van Breugel (San Fransicso: ASP), 525
Pettini, M. 2001, ApJ, 554, 981
Pettini, M., Kellogg, M., Steidel, C. C., Dickinson, M. E., Adelberger, K. L., & Giavalisco, M. 1998, ApJ, 508, 539
Phillips, S., Parker, Q. A., Schwartzenberg, J. M., & Jones, J. B. 1998, ApJ, 493, L59
Renzini, A. 1997, ApJ, 488, 35
Scannapieco, E., & Broadhurst, T. 2001, ApJ, 549, 28 (SB)
Scannapieco, E., Ferrara, A., & Broadhurst, T. 2000, ApJ, 526, L11
Shopbell, P. L., & Bland-Hawthorn, J. 1998, ApJ, 493, 129
Smecker-Hane, T. A., Stetson, P. B., Hesser, J. E., & Lehnert, M. D. 1994, AJ, 108, 507
Spergel, D., & Steinhardt, P. J. 2001, Phys. Rev. Lett., 84, 3760
Springel, V. 2000, MNRAS, 312, 859
Steidel, C. C., Adelberger, K. A., Giavalisco, M., Dickinson, M., & Pettini, M. 1999, ApJ, 519, 1
Sutherland, R. S., & Dopita, M. A. 1993, ApJS, 88, 253
Sunyaev, R. A., & Zel'dovich, Ya. B. 1972, Comments Astrophys. Space Phys., 4, 173
Tegmark, M., Silk, J., & Evrard, A. 1993, 417, 54
Thacker, R. J., & Couchman, H. M. P. 2000, ApJ, 545, 728
Thacker, R. J., & Davis, M. 1999, in ASP Conf. Ser. 193, The Hy-Redshift Universe: Galaxy Formation at High Redshift, ed. A. J. Bunker & W. J. M. van Breugel (San Fransicso: ASP), 353
Thacker, R. J., Tittley, E. R., Pearce, F. R., Couchman, H. M. P., & Thomas, P. A. 2000, MNRAS, 319, 619
Thomas, P. A., & Couchman, H. M. P. 1992, MNRAS, 257, 11
Thornton, K., Gaulditz, M., Janka, H.-Th., & Steinmetz, M. 1998, ApJ, 500, 95
Trentham, N., Möller, O., & Ramirez-Ruiz, E. 2001, MNRAS, 322, 658
Warren, S. J., Iovino, A., Hewett, P. C., & Shaver, P. A. 1998, MNRAS, 299, 215
Yepes, G., Kates, R., Khokhlov, A., & Klypin A. 1997, MNRAS, 284, 235
Zel'dovich Ya. B., & Sunyaev, R. A. 1969, Ap&SS, 4, 301